Arris S. Tijsseling
Department of Mathematics
and Computer Science,
Eindhoven University of Technology,
P.O. Box 513,
Eindhoven 5600 MB, The Netherlands
e-mail: a.s.tijsseling@tue.nl

Qingzhi Hou[1]
School of Computer Science
and Technology,
State Key Laboratory of Hydraulic Engineering,
Simulation and Safety,
Tianjin University,
Tianjin 300072, China
e-mail: qhou@tju.edu.cn

Zafer Bozkuş
Hydromechanics Laboratory,
Department of Civil Engineering,
Middle East Technical University,
Ankara 06800, Turkey
e-mail: bozkus@metu.edu.tr

Janek Laanearu
Department of Mechanics,
Tallinn University of Technology,
Tallinn 19086, Estonia
e-mail: janek.laanearu@ttu.ee

Improved One-Dimensional Models for Rapid Emptying and Filling of Pipelines

Improved one-dimensional (1D) models—compared to previous work by the authors—are proposed which are able to predict the velocity, length, and position of the liquid column in the rapid emptying and filling of a pipeline. The models include driving pressure and gravity, skin friction and local drag, and holdup at the tail and gas intrusion at the front of the liquid column. Analytical and numerical results are validated against each other, and against experimental data from a large-scale laboratory setup.
[DOI: 10.1115/1.4031508]

Keywords: pipe flow, filling, priming, emptying, draining, holdup, air intrusion, analytical solution

Introduction

Long liquid slugs traveling in pipelines and separated by gas pockets involve a risk that needs to be assessed. These slugs inevitably occur in pipe emptying and filling operations. In pipe emptying an initially very long slug finally becomes very short, and in pipe filling it is vice versa. Short slugs may accelerate to high velocities and impose serious impact forces on the pipe system when hitting obstacles like bends and valves. The impact force is proportional to the square of the slug's speed, and the impact duration is proportional to the slug's length and inversely proportional to its speed [1]. Damage typically happens to pipe anchors and hydraulic machinery. A good prediction of slug speeds and slug lengths is essential in risk and postaccident analyses.

Previous work on the subject has been reviewed in Refs. [2–4]. The current improvement in one-dimensionally modeling pipe emptying and filling [5] is that liquid holdup and gas intrusion [6] are included, and that therefore the velocity of the liquid column is *not* taken uniform in the flow direction, because front and tail move at different speeds. The three governing equations for velocity, length, and position are coupled and strongly nonlinear, yet a range of analytical solutions is derived. The obtained analytical and numerical solutions are compared with laboratory measurements [3,4].

Pipe-Emptying Model and Solution

Consider the schematized liquid-column (indicated as slug) moving at speed v in a straight pipe as sketched in Fig. 1. The outflow is at constant position x_1 and the planar tail is at changing position x_2. The pressure is P_1 at the outflow and P_2 ($>P_1$) at the tail. The slug has mass m, length L, and constant density ρ related by

$$m = \rho A L \tag{1}$$

The moving liquid-column loses mass at a rate proportional to the distance traveled and leaves behind a liquid layer—the *holdup*—occupying a constant fraction βA of the pipe cross-sectional area A, with $0 \leq \beta < 1$. The slug length $L = x_1 - x_2$ decreases from pipe length x_L to zero (theoretically).

Conservation of Mass. The mass balance for the shortening rigid-column is (Fig. 1)

$$\frac{\mathrm{d}}{\mathrm{d}t}\int_{x_2(t)}^{x_1} \rho A \,\mathrm{d}x = -\rho A\, v_1(t) - \rho A\, \beta \frac{\mathrm{d}x_2}{\mathrm{d}t}(t) \tag{2}$$

which directly leads to

$$-\frac{\mathrm{d}x_2}{\mathrm{d}t}(t) = -v_1(t) - \beta \frac{\mathrm{d}x_2}{\mathrm{d}t}(t) \;\text{ or }\; v_1(t) = (1-\beta)\, v_2(t), \quad \text{where } v_2 = \frac{\mathrm{d}x_2}{\mathrm{d}t} \tag{3}$$

The slug length is

$$L(t) = x_1 - x_2(t) = L_0 - (x_2(t) - x_2(t_0)) \tag{4}$$

with the constant $L_0 := x_1 - x_2(t_0)$.

In terms of v_2 and L, the governing equation is

$$\frac{\mathrm{d}L}{\mathrm{d}t}(t) = -v_2(t) \tag{5}$$

[1]Corresponding author.

Contributed by the Pressure Vessel and Piping Division of ASME for publication in the Journal of Pressure Vessel Technology. Manuscript received March 23, 2015; final manuscript received August 23, 2015; published online December 10, 2015. Assoc. Editor: Jong Chull Jo.

Conservation of Momentum. The momentum balance (that is consistent with the moving mass balance) is

$$\frac{\mathrm{d}}{\mathrm{d}t}\int_{x_2(t)}^{x_1}\rho A\, v(x,t)\,\mathrm{d}x = -\rho A\, v_1^2(t) - \rho A\,\beta\,\left(v_2(t) - v_{\mathrm{hu}}(t)\right)\frac{\mathrm{d}x_2}{\mathrm{d}t}(t) + \left(P_2(t) - P_1(t)\right)A + \int_{x_2(t)}^{x_1}\rho A\, g\,\sin\theta(x)\,\mathrm{d}x - \frac{f}{2D}\int_{x_2(t)}^{x_1}\rho A\, v^2(x,t)\,\mathrm{d}x - \frac{K}{2}\,\rho A\, v_1^2(t) \tag{6}$$

where $v_{\mathrm{hu}}(t)$ is the velocity of the holdup directly behind the tail, g is the acceleration due to gravity, θ is the angle of the pipe's downward inclination, f is the (skin) friction factor according to Darcy–Weisbach, and the last term represents resistance (drag) at the exit (at x_1) with loss coefficient K. The unknown force F_{hu} creating the holdup is ignored. For the sake of simplicity, and because it is an unknown factor, $v_{\mathrm{hu}}(t)$ is taken zero herein, i.e., the holdup sticks to the pipe wall. Applying Leibniz's rule results (with $v_{\mathrm{hu}} \equiv 0$) in

$$-v\left(x_2^+(t),t\right)\frac{\mathrm{d}x_2}{\mathrm{d}t}(t) + \int_{x_2(t)}^{x_1}\frac{\partial v}{\partial t}(x,t)\,\mathrm{d}x = -v_1^2(t) - \beta\, v_2^2(t) + \frac{P_2(t) - P_1(t)}{\rho} + g\int_{x_2(t)}^{x_1}\sin\theta(x)\,\mathrm{d}x - \frac{f}{2D}\int_{x_2(t)}^{x_1} v^2(x,t)\,\mathrm{d}x - \frac{K}{2}\,v_1^2(t) \tag{7}$$

Rearranging gives [using Eq. (3)]

$$\begin{aligned}\int_{x_2(t)}^{x_1}\frac{\partial v}{\partial t}(x,t)\,\mathrm{d}x - \frac{P_2(t) - P_1(t)}{\rho} - g\int_{x_2(t)}^{x_1}\sin\theta(x)\,\mathrm{d}x &= -v_1^2(t) + (1-\beta)\, v_2^2(t) - \frac{f}{2D}\int_{x_2(t)}^{x_1} v^2(x,t)\,\mathrm{d}x - \frac{K}{2}\,v_1^2(t)\\ &= \beta\,(1-\beta)\, v_2^2(t) - \frac{f}{2D}\int_{x_2(t)}^{x_1} v^2(x,t)\,\mathrm{d}x - \frac{K}{2}\,(1-\beta)^2\, v_2^2(t)\end{aligned} \tag{8}$$

The three integrals are evaluated in the Appendix. In terms of v_2 and L, the governing equation becomes (using Eqs. (A1)–(A3))

$$\left(1 - \frac{1}{2}\beta\right)L(t)\,\frac{\mathrm{d}v_2}{\mathrm{d}t}(t) = \beta\,(1-\beta)\, v_2^2(t) + \frac{P_2(t) - P_1(t)}{\rho} + g\left[z(x_2(t)) - z(x_1)\right] - \frac{f}{2D}\left(1 - \beta + \frac{1}{3}\beta^2\right)L(t)\, v_2^2(t) - \frac{K}{2}\,(1-\beta)^2\, v_2^2(t) \tag{9}$$

where z is the elevation of the pipeline.

Note: The first term on the right represents a self-propelling mechanism, because the control volume (CV) loses mass at its tail. It is consistent with the corresponding term in Eq. (28) for pipe filling, but with the essential difference that the CV taken to model pipe filling does *not* lose mass.

The linearly distributed pressure in the rigid liquid column ($x > x_2(t)$) and in the driving gas ($x < x_2(t)$) are given by

$$P(x,t) = \begin{cases} P_2(t) \text{ if } 0 \le x < x_2(t) \\ P_1(t) + \dfrac{K}{2}\rho(1-\beta)^2 v_2^2(t) + \dfrac{x_1 - x}{L(t)}\left(P_2(t) - P_1(t) - \dfrac{K}{2}\rho(1-\beta)^2 v_2^2(t)\right) \text{ if } x_2(t) \le x \le x_1 = x_L \end{cases} \tag{10}$$

Analytical Solution. An analytical solution can be derived for v_2 when both the pressure difference $P_2 - P_1 > 0$ and the pipe slope $\theta > 0$ are constant ($\theta < 0$ is also allowed as long as the flow does not reverse). Equation (5) is used to eliminate v_2 from Eq. (9), so that

$$L\,\frac{\mathrm{d}^2L}{\mathrm{d}t^2} = -\frac{\beta\,(1-\beta)}{1 - \frac{1}{2}\beta}\left(\frac{\mathrm{d}L}{\mathrm{d}t}\right)^2 - \frac{1}{1 - \frac{1}{2}\beta}\,\frac{P_2 - P_1}{\rho} - \frac{g\,L\,\sin\theta}{1 - \frac{1}{2}\beta} + \frac{f}{2D}\,\frac{1 - \beta + \frac{1}{3}\beta^2}{1 - \frac{1}{2}\beta}\,L\left(\frac{\mathrm{d}L}{\mathrm{d}t}\right)^2 + \frac{K}{2}\,\frac{(1-\beta)^2}{1 - \frac{1}{2}\beta}\left(\frac{\mathrm{d}L}{\mathrm{d}t}\right)^2 \tag{11}$$

Define $\dfrac{\mathrm{d}L}{\mathrm{d}t} := w(L) \;\; < 0$, $\gamma := \dfrac{2\,\beta\,(1-\beta)}{1 - \frac{1}{2}\beta} - \dfrac{K\,(1-\beta)^2}{1 - \frac{1}{2}\beta}$, $\tilde{f} := \dfrac{f}{2\,D}\,\dfrac{1 - \beta + \frac{1}{3}\beta^2}{1 - \frac{1}{2}\beta}$, and note that

$$\frac{\mathrm{d}^2L}{\mathrm{d}t^2} = \frac{\mathrm{d}w}{\mathrm{d}t} = \frac{\mathrm{d}w}{\mathrm{d}L}\,\frac{\mathrm{d}L}{\mathrm{d}t} = w\,\frac{\mathrm{d}w}{\mathrm{d}L} = \frac{1}{2}\,\frac{\mathrm{d}w^2}{\mathrm{d}L} \tag{12}$$

The following linear first-order ordinary differential equation (ODE) in w^2 is derived

$$\frac{\mathrm{d}w^2}{\mathrm{d}L} + \left(\frac{\gamma}{L} - 2\tilde{f}\right)w^2 = -\frac{2}{1 - \frac{1}{2}\beta}\,\frac{P_2 - P_1}{\rho\,L} - \frac{2}{1 - \frac{1}{2}\beta}\,g\,\sin\theta \tag{13}$$

The solution for the initial condition $v_2(t_0) = 0$ or $w(L_0) = 0$ is obtained after multiplying Eq. (13) with the integrating factor $L^{\gamma}\,\mathrm{e}^{2\tilde{f}L}$

$$w^2 = \frac{2}{1 - \frac{1}{2}\beta}\,\frac{P_2 - P_1}{\rho}\left(\Gamma^*(L) - \Gamma^*(L_0)\left(\frac{L_0}{L}\right)^{\gamma}\right)\mathrm{e}^{2\tilde{f}L} + \frac{2}{1 - \frac{1}{2}\beta}\,g\,\sin\theta\,L\left(\frac{\Gamma\left(\gamma+1,\,2L\tilde{f}\right)}{\left(2L\tilde{f}\right)^{\gamma+1}} - \frac{\Gamma\left(\gamma+1,\,2L_0\tilde{f}\right)}{\left(2L_0\tilde{f}\right)^{\gamma+1}}\left(\frac{L_0}{L}\right)^{\gamma+1}\right)\mathrm{e}^{2\tilde{f}L} \tag{14}$$

with

$$\Gamma^*(L) := \frac{1}{\gamma}\left(\frac{\Gamma\left(\gamma+1,\,2L\tilde{f}\right)}{\left(2L\tilde{f}\right)^{\gamma}} - \mathrm{e}^{-2\tilde{f}L}\right).$$

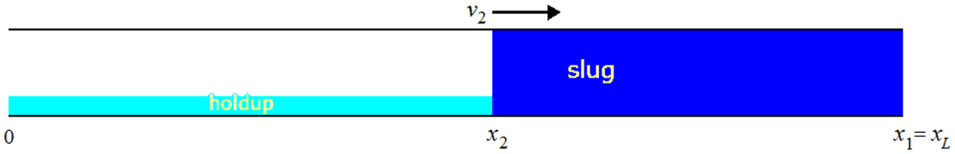

Fig. 1 Sketch of pipe emptying. CV = slug = volume between x_2 and x_1.

Γ is the upper incomplete gamma function. If $\gamma + 1 < 0$ integrations by parts are needed to obtain a valid analytical solution. The slug length L is replaced by $L_0 - L_{\text{pipe}}$, according to Eq. (4), where $L_{\text{pipe}} := x_2(t) - x_2(t_0)$ is the distance traveled by the tail of the liquid column. This notation is adapted from Ref. [1]. The symbolic formula for v_2 (instead of w^2) as function of L_{pipe} follows then directly from Eqs. (5) and (14). The special—or limiting—case $f = 0$ gives the solution

$$v_2 = \sqrt{\frac{2}{1 - \frac{1}{2}\beta}} \sqrt{\frac{P_2 - P_1}{\rho\,\gamma}\left(\left(\frac{L_0}{L}\right)^{\gamma} - 1\right) + \frac{2\,g\,\sin\theta}{\gamma + 1} L \left(\left(\frac{L_0}{L}\right)^{\gamma+1} - 1\right)} \tag{15}$$

For the case $\beta = 0$ and $K = 0$ (and hence $\gamma = 0$) the solution is

$$v_2 = \sqrt{2\,\frac{P_2 - P_1}{\rho}\,\mathrm{e}^{2C_2 L}\left(\mathrm{Ei}(-2C_2 L_0) - \mathrm{Ei}(-2C_2 L)\right) + \frac{g\,\sin\theta}{C_2}\left(1 - \mathrm{e}^{-2C_2(L_0 - L)}\right)} \tag{16}$$

where $C_2 := f/2D$ and the difference of exponential integrals Ei in the first term is herein calculated numerically according to

$$\mathrm{Ei}(-2C_2 L_0) - \mathrm{Ei}(-2C_2 L) = \int_L^{L_0} \frac{\mathrm{e}^{-2C_2 L^*}}{L^*}\,\mathrm{d}L^* \tag{17}$$

Numerical Solution. Numerical integration is required when the pressure difference $P_2 - P_1$ is not constant but given by measured or calculated (using gas dynamics) values. It is also required when the pipe slope θ is not constant. The governing Equations (9) and (5) and $(\mathrm{d}x_2/\mathrm{d}t)(t) = v_2(t)$ can be casted in the standard form

$$\frac{\mathrm{d}\boldsymbol{y}}{\mathrm{d}t} = \boldsymbol{f}(t, \boldsymbol{y}),\ \text{with}\ \boldsymbol{y} := \begin{pmatrix} v_2 \\ L \\ x_2 \end{pmatrix} \tag{18}$$

The explicit Euler method is used herein to solve Eq. (18), but any suitable numerical integration scheme can do the job.

Pipe-Emptying Validation

Test Problem. The experimental setup described in Ref. [3]—a pipeline filled with water and connected to a tank with compressed air—is used as test problem for pipe emptying. The pipeline consists of 275.2 m of PVC pipe connected upstream and downstream to steel pipes with lengths 29.1 m and 9.8 m, respectively, giving a total length of 314.1 m. A dead-end sidebranch is ignored. The PVC and steel pipes have diameters of 0.2354 m and 0.206 m, respectively. Herein an average diameter of 0.232 m is taken, such that the volume of the actual and averaged pipeline is the same. The PVC pipe contains a 6.5-m-long 1.3-m-high bridge at its upstream end. The upstream and downstream steel pipes contain 1.2 m and 4.0 m vertical sections, respectively. The chosen coordinate (x) along the pipeline ($-43.1\,\text{m} \le x \le 271.0\,\text{m}$) and the corresponding vertical elevation (z), with $z(x_1) = -4\,\text{m}$, are depicted in Fig. 2. The upstream boundary is a check valve that separates water and air (V7 in Ref. [4]) and the downstream boundary is a control valve (V4 in Ref. [4]). A second downstream valve (V5 in Ref. [4]) discharging to the open atmosphere, and located 0.6 m below V4, is initially closed (see Fig. 3). Compressed air from an upstream tank keeps the water column pressurized. It is assumed—but this could not be verified directly—that water occupies the pipeline up to the check valve at $x = -43.1$ m. Rapid opening of valve V5 at $t_0 = 0$ initiated the draining. This caused an acoustic decompression wave (waterhammer) which is ignored herein. Valve V4 was set at different positions in different runs. The input parameters for the numerical simulation are listed in Table 1 and directly taken from Ref. [3]. The holdup factor β is taken constant herein (with values between 0.2 and 0.3), although the holdup changes with time [7] (see Fig. 5 in Ref. [3]). A value of 0.3 for β corresponds to a water depth h of 0.08 m, so that $h/D = 0.34$ (see Fig. 4). Minor losses at pipe bends are partly included in the friction factor f. The pressure in the air tank was not constant during the draining process, but decreased gradually and roughly linearly. The downstream pressure $P_1(t) \equiv 0$ is atmospheric.

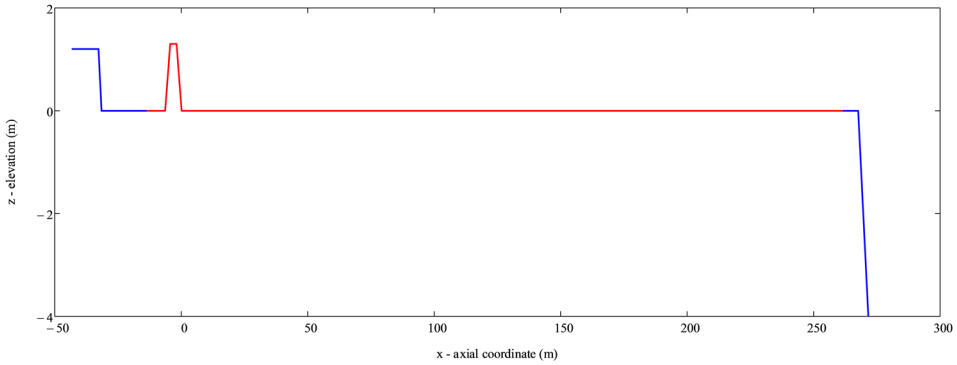

Fig. 2 Pipeline axial coordinates and elevation profile $z(x)$ for pipe emptying [3]; not to scale

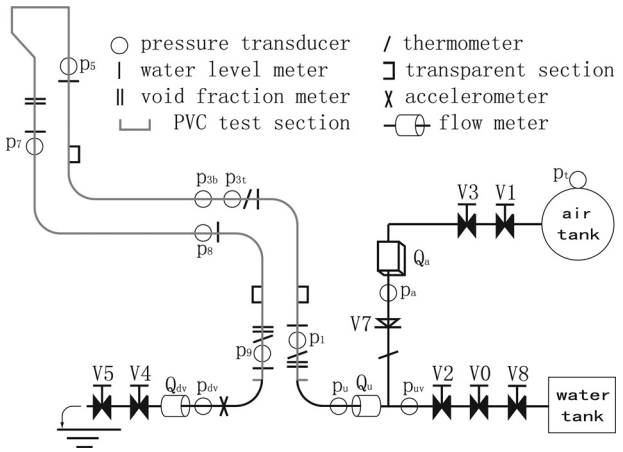

Fig. 3 Positions of valves, pressure transducers, and flowmeters in experimental apparatus; not to scale

Results

All analytical solutions have been successfully verified against numerical results and vice versa (not shown).

Nine experimental runs were reported in Ref. [3] in which the driving air pressure (with initial head H_0), its linearized decay (dH/dt), the partial closing of the control valve V4 (K_e), and the holdup coefficient (β) varied according to the values given in Table 2. One additional experimental run (run 0) has been added here in which the draining is solely by gravity ($\Delta P(t) \equiv 0$) and the downstream valves are fully open.

The values for the holdup coefficient β are determined from the measured difference of pipeline volume and discharged volume up to the time that the air–water front arrives at the downstream electromagnetic flowmeter (EMF), because this is exactly the volume of water that is left behind in the pipeline. The volume of the pipeline and its initial water column is $V_0 = 13.3\ \text{m}^3$ and the discharged volume is $\int_0^{t(x_{\text{EMF}})} Q(t)\,dt$. If the difference (the leftover) is homogeneously distributed along the pipeline that gives a constant value $\beta = 1 - (1/V_0)\int_0^{t(x_{\text{EMF}})} Q(t)\,dt$. For runs 1 to 9 these values are given in Table 2.

The initial acceleration from rest according to Eq. (9) is

$$\psi \frac{dv_2}{dt}(t_0) = \frac{P_2(t_0)}{\left(1 - \frac{1}{2}\beta\right)\rho L_0} + \frac{g\left[z(x_2(t_0)) - z(x_1)\right]}{\left(1 - \frac{1}{2}\beta\right) L_0} \tag{19}$$

Table 1 Input data for pipe-emptying simulations

Input parameters	Notation	Values
Length of pipeline	x_L	314.1 m
Average diameter of pipeline	D	0.232 m
Mass density of water	ρ	998.5 kg/m^3
Gravitational acceleration	g	9.81 m/s^2
Friction factor (PVC pipe)	f	0.0136
End loss coefficient	K	3.3 – 22.7
Holdup coefficient	β	0.23 – 0.29, see Table 2
Driving pressure	$\Delta P(t)$	1 – 2 barg, see Table 2
Elevation profile	$z(x)$	see Fig. 2
Derived quantities	**Notation**	**Values**
Flow area	A	0.0423 m^2
Initial mass	m_0	13254 kg
$f/(2D)$	C_2	0.0293 1/m

where ψ is an unsteady friction coefficient ($1 \le \psi \le 4/3$) discussed at the end of this section and the initial difference in elevation between air–water front and outflow location is $z(x_2(t_0)) - z(x_1) = 5.2\,\text{m}$. When there is no driving pressure ($P_2(t) \equiv 0$) as in run 0, the acceleration starts at 0.19 m/s^2, and then decreases mainly because of skin friction. This is shown in Fig. 5, together with the retarding effect of $\psi > 1$. The acceleration corresponds to the elevation profile (Fig. 2) and increases monotonically after 26 s, simply because the liquid column (slug) becomes shorter. When there is a driving pressure, as in run 4, the pressures measured and calculated at Secs. 1 ($x = 1.55\,\text{m}$) and 9 ($x = 252.8\,\text{m}$) are shown in Fig. 6. The sudden opening of valve V5 at $z = -4.6\,\text{m}$ makes the local pressure-head drop from $H_0 + 1.2\,\text{m} - z = 25.9\,\text{m}$ to zero (atmospheric). This zero pressure-head travels upstream as an acoustic wave and has gradually dropped to $-4.6\,\text{m}$ when it reaches the horizontal pipeline at reference elevation $z = 0$. This explains the 0.4 bar negative pressure measured at Sec. 9. The subsequent peaks are due to reflections from the compressed air upstream. Waterhammer is ignored in the numerical simulations, where the liquid column is rigid (not elastic). The smooth lines are based on Eq. (10) and the calculated velocity v_2. Exactly at the instant when the signals of Secs. 1 and 9 meet, the slug tail has reached Sec. 9 and both transducers (at 9 and 1) measure air pressure. This instant is predicted too late by the simulation. The time $\tau_{(1)–(9)}$ taken by the slug tail to travel from Secs. 1 to 9 is listed in Table 2 together with the tail's instantaneous speeds. The measured and calculated travel times $\tau_{(1)–(9)}$ differ less than 10% and the same holds for the tail velocities at Sec. 1, except for runs 2 and 3. The measured and calculated velocities at Sec. 9 differ less than 5%.

The measured and calculated outflow discharges are displayed in Fig. 7. The measured curves end when the first air arrives at the EMF positioned at $x = 269.8\,\text{m}$. The discharged volume is the area under a curve. The main conclusion is that all trends are correct if the initial waterhammer (the stepwise increase of flow rate) is disregarded. Applying the Joukowsky formula (for waterhammer) to estimate the first step-increase of the flow rate gives $\Delta Q = g A\,\Delta H / a = 0.029\ \text{m}^3/\text{s}$, where $\Delta H = 24.7\,\text{m}$ and the PVC pipeline's measured pressure wave speed $a = 348\,\text{m/s}$ [8]. This value compares well with a recorded step of 0.033 m^3/s in Fig. 7(*a*). The 10.4 m of steel pipe leading to the PVC pipe has an estimated wave speed larger than 1200 m/s [8], a travel time less than 10 ms, and therefore not a big influence on the waterhammer event in the PVC pipeline [9].

The initial slug length L_0 could not be detected directly. Three different ways of estimating it indirectly are based on: (1) initial average acceleration according to Eq. (19); (2) initial waterhammer travel time $\tau_{\text{wh},0} = 2L_0/a$; and (3) initial waterhammer frequency $f_0 = a/(2L_0)$.

The acceleration $dv_2/dt(t_0)$ for a driving pressure of 2 barg (runs 1, 4, 5, and 6) as estimated from the rate of change of the outflow

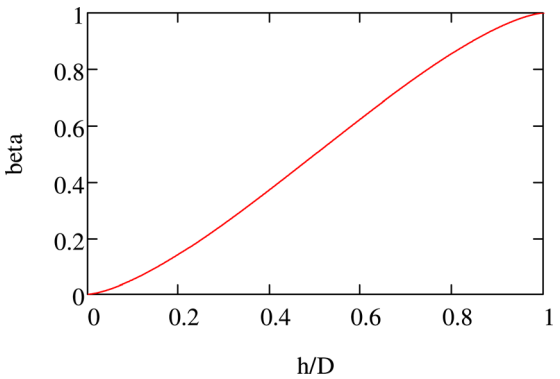

Fig. 4 Holdup coefficient β as function of dimensionless water depth h/D in a circular pipe

Table 2 Main results for pipe emptying

Run (No.)	H_0 (m)	dH/dt (m/s)	K[a]	β	Measured $\tau_{(1)–(9)}$ (s)	Calculated $\tau_{(1)–(9)}$ (s)	Measured[a,b] $v_{2(1)}$ (m/s)	Calculated $v_{2(1)}$ (m/s)	Measured[a,c] $v_{2(9)}$ (m/s)	Calculated $v_{2(9)}$ (m/s)
1	19.60	−0.114	3.32	0.24	37	37	6.0	5.4	11.3	11.4
2	14.90	−0.0815	3.50	0.25	45	41	4.0	4.8	10.1	10.2
3	9.80	−0.051	3.48	0.27	51	47	3.3	4.2	8.9	9.0
4	20.10	−0.119	3.64	0.24	36	37	6.0	5.4	11.6	11.2
5	20.00	−0.105	5.88	0.23	40	39	5.8	5.2	9.9	9.3
6	19.65	−0.063	21.24	0.26	54	52	4.9	4.4	5.9	5.6
7	10.05	−0.058	3.84	0.26	46	48	4.6	4.2	9.1	8.5
8	10.00	−0.051	6.14	0.27	50	50	4.4	4.1	7.7	7.3
9	9.80	−0.033	22.68	0.29	69	68	3.6	3.4	4.4	4.3
0	0	0	3.5	0.29	—	79	—	2.4	—	5.6
						81[d]		2.3[d]		5.5[d]

[a]Based on $D = 0.2354$ m, which means that for $D = 0.232$ m (used herein) K should be a factor 1.03 smaller and the measured velocities should be a factor 1.03 larger.
[b]$v_{2(1)} = v_1/(1-\beta)$, where v_1 is the measured outflow velocity [3] and $v_{2(1)}$ is the tail's velocity when it arrives at Sec. 1.
[c]$v_{2(9)} = v_1/(1-\beta)$, where v_1 is the measured outflow velocity [3] and $v_{2(9)}$ is the tail's velocity when it arrives at Sec. 9.
[d]$\psi = 4/3$ (see Fig. 5).

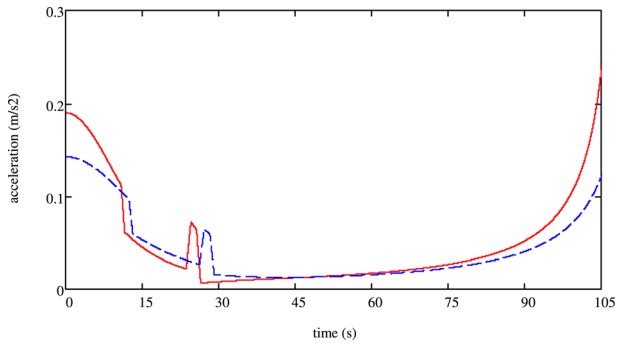

Fig. 5 Simulated acceleration during gravity draining ($\Delta P = 0$): $\psi = 1$ (continuous line) and $\psi = 4/3$ (discontinuous line)

discharge $(1/A\,\Delta Q/\Delta t)(t_0) = (1/0.0423)(0.15/5) = 0.71$ m/s^2. Substituting this value and $z(x_2(t_0)) - z(x_1) = 5.2$ m in Eq. (19) gives $L_0 = \frac{H_0+5.2\,\rho\,g}{1-\frac{1}{2}\beta}\,\frac{g}{\frac{dv_2}{dt}(t_0)}$ and an estimate $L_0 = 397$ m for run 4. For a driving pressure of 1 barg (runs 3, 7, 8, and 9), the estimated initial acceleration is $(1/A\,\Delta Q/\Delta t)(t_0) = (1/0.0423)(0.14/10) = 0.33$ m/s^2. Substituting this value in Eq. (19) gives an estimate $L_0 = 521$ m for run 7. These values are obviously much too large, which is consistent with the too large initial accelerations seen in Fig. 7(*b*). Also, the initial acceleration in the experiment cannot be determined accurately because of the hydraulic transients (waterhammer). However, the waterhammer can be used to estimate the

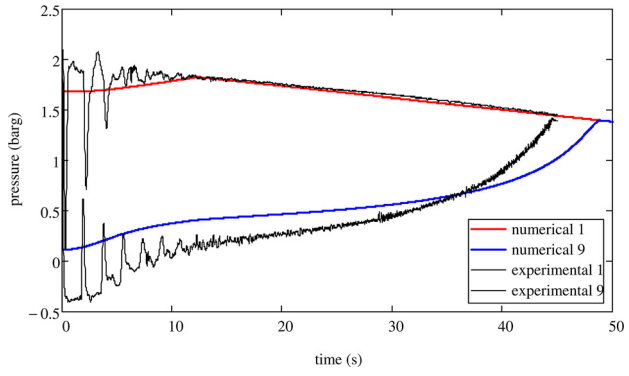

Fig. 6 Pressure histories at measurement Sections 1 and 9 for emptying run 4 (repetition 2): measured (whimsical lines) [3] and calculated (smooth lines) histories

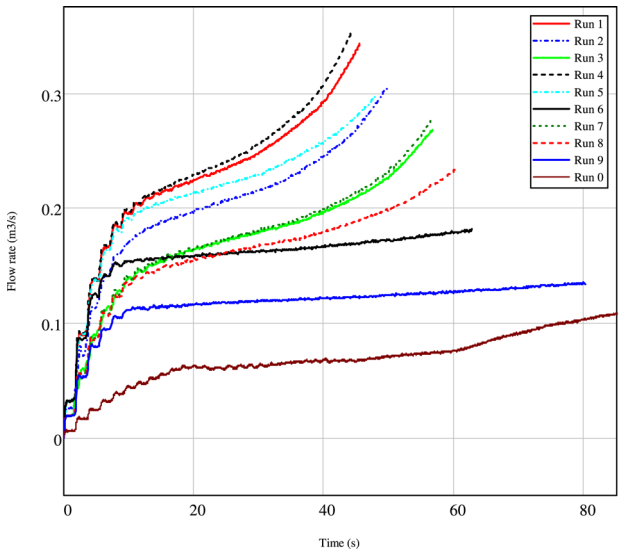

(*a*)

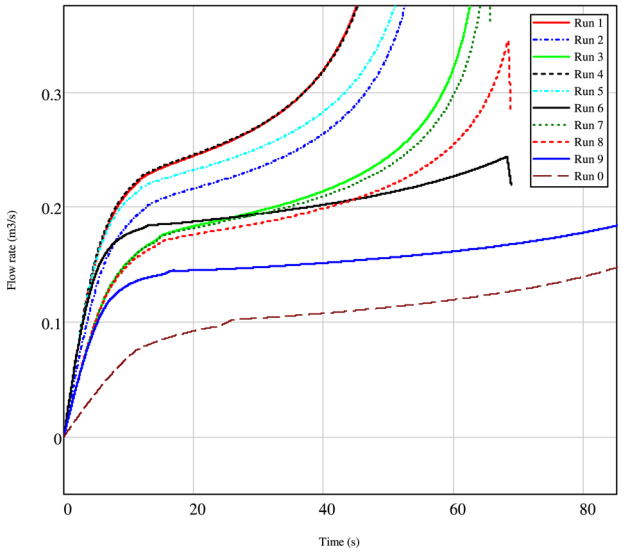

(*b*)

Fig. 7 Outflow discharges for pipe emptying: (*a*) measurements [3] and (*b*) calculations

column length. The first return time of the reflected pressure wave detected from Fig. 7(*a*) is $\tau_{wh,0}=1.85$ s. This gives an estimate of $L_0=322$ m, which is a little above the maximum possible length of 314 m. The initial waterhammer frequency, shown by Fig. 10 in Ref. [3], is $f_0=0.62$ Hz. This leads to an estimate of $L_0=281$ m, which is 33 m less than the maximum possible length. The average of the two different waterhammer estimates is 301 m, which is consistent with the chosen L_0 in Table 1. The estimates of L_0 based on the waterhammer concern the sudden start of the acceleration and seem all right in view of the limited accuracy of the measurements. The theoretical initial accelerations based on Eq. (19) are systematically too high and ask for an explanation, possibly unsteady friction [10–14]. Unsteady laminar friction may result in an apparent increase of inertia by a factor $\psi=4/3$ [15], which leads to the more appropriate estimates of 298 m (run 4) and 391 m (run 7) for L_0. It may take several seconds before a fully developed turbulent flow is established, but this issue is not pursued herein.

Pipe-Filling Model and Solution

Consider the schematized liquid-column (indicated as slug) moving at speed v in a straight pipe as sketched in Fig. 8. The inflow is at constant position x_2 and the planar front is at changing position x_1. The pressure is P_2 at the inflow and P_1 ($<P_2$) at the front.

The moving liquid-column takes in air (at its front) occupying a constant fraction βA of the pipe cross-sectional area A, with $0 \le \beta < 1$. The (gravity driven) air front propagates with constant speed c relative to the slug front, as displayed in Fig. 8. The slug length $L = x_1 - x_2$ increases from $L_0 > 0$ to pipe length x_L. Note that $dx_1/dt = v_1$, but that $dx_2/dt = 0 \neq v_2 = v(x_2)$ and $dx_3/dt \neq v_3 = v(x_3)$, because v is discontinuous at the secondary water–air front at x_3 (it jumps from v_2 to v_1) and therefore flow velocity v_3 is not defined. In fact, there are two rigid-columns: one with velocity v_2 upstream of x_3 and one with velocity $v_1 > v_2$ downstream of x_3 (Fig. 8). The moving jump at x_3 makes this possible.

Conservation of Mass. The mass balance is

$$\frac{d}{dt}\int_{x_2}^{x_1(t)} \rho A_l(x,t)\,dx = \rho A\, v_2(t) \tag{20}$$

where A_l is the cross-sectional flow area of the liquid. Separating (at x_3) the two regions sketched in Fig. 8 gives

$$\frac{d}{dt}\int_{x_2}^{x_3(t)} \rho A\,dx + \frac{d}{dt}\int_{x_3(t)}^{x_1(t)} \rho(1-\beta)A\,dx = \rho A\, v_2(t) \tag{21}$$

Downstream of x_3, either the flow area (in Eq. 20) or the fluid density (not necessarily stratified flow), is reduced by a factor $1-\beta$ (in Eq. 21); this depends on the chosen CV which herein precisely surrounds the liquid. Take the derivatives of the integrals to find

$$\frac{dx_3}{dt}(t) + (1-\beta)\left(\frac{dx_1}{dt}(t) - \frac{dx_3}{dt}(t)\right) = v_2(t) \quad \text{or} \quad (1-\beta)\,v_1(t) + \beta\frac{dx_3}{dt}(t) = v_2(t) \tag{22}$$

with $dx_3/dt(t) = v_1(t) - c$ (by definition) so that

$$v_2(t) = v_1(t) - \beta c \tag{23}$$

Note that $v_1(t) = \beta c$ for a closed upstream end. The value of c is estimated by [16]

$$c = \sqrt{g\,\cos\theta\,\frac{(1-\beta)A}{T}} \tag{24}$$

where T is the top width of the prismatic flow section, $g\cos\theta$ is the y-component of gravitational acceleration perpendicular to the x-direction. The speed c is $\sqrt{gh}$ when the angle of pipe inclination $\theta=0$ and the dimensionless flow depth h/D (a function of β) equals 0.769 [4]. The speed c tends to infinity when h/D approaches unity.

Conservation of Momentum. The momentum balance is (assuming that $P_3(\text{air}) = P_1$)

$$\frac{d}{dt}\int_{x_2}^{x_1(t)} \rho A_l(x,t)\,v(x,t)\,dx = \rho A\, v_2^2(t) + (P_2(t) - P_1(t))A + \int_{x_2}^{x_1(t)} \rho A_l\, g\,\sin\theta(x)\,dx - \frac{1}{2D}\int_{x_2}^{x_1(t)} f\rho A_l(x,t)\,v^2(x,t)\,dx - \frac{K}{2}\rho A\, v_2^2(t) \tag{25}$$

where the unknown force needed to "drive the air upstream" (F_{air}) is entirely ignored, so that after separation at x_3

$$\begin{aligned}\frac{d}{dt}\int_{x_2}^{x_3(t)} \rho A\,v(x,t)\,dx + \frac{d}{dt}\int_{x_3(t)}^{x_1(t)} \rho(1-\beta)A\,v(x,t)\,dx \\ = \rho A\, v_2^2(t) + (P_2(t) - P_1(t))\,A + \int_{x_2}^{x_3(t)} \rho A g\,\sin\theta(x)\,dx \\ + \int_{x_3(t)}^{x_1(t)} \rho A(1-\beta) g\,\sin\theta(x)\,dx - \frac{f_2}{2D}\int_{x_2}^{x_3(t)} \rho A\,v^2(x,t)\,dx \\ - \frac{f_1}{2D_H}\int_{x_3(t)}^{x_1(t)} \rho(1-\beta)A\,v^2(x,t)\,dx - \frac{K}{2}\rho A\, v_2^2(t)\end{aligned} \tag{26}$$

where $D_H = 4A_l/P_l$ is the hydraulic diameter and P_l is the wetted perimeter. Apply Leibniz's rule to arrive at

$$\begin{aligned}v\left(x_3^-(t),t\right)\frac{dx_3}{dt}(t) + \int_{x_2}^{x_3(t)} \frac{\partial v}{\partial t}(x,t)\,dx \\ + (1-\beta)\left(v(x_1(t),t)\frac{dx_1}{dt}(t) - v\left(x_3^+(t),t\right)\frac{dx_3}{dt}(t)\right) \\ + (1-\beta)\int_{x_3(t)}^{x_1(t)} \frac{\partial v}{\partial t}(x,t)\,dx = v_2^2(t) + \frac{P_2(t) - P_1(t)}{\rho} \\ + g\left[z(x_2) - z(x_3(t))\right] + (1-\beta)\,g\left[z(x_3(t)) - z(x_1(t))\right] \\ - \frac{f_2}{2D}(x_3(t) - x_2)\,v_2^2(t) - \frac{f_1}{2D_H}(x_1(t) - x_3(t))\,(1-\beta)\,v_1^2(t) \\ - \frac{K}{2}\rho A\, v_2^2(t)\end{aligned}$$

or, using $x_1 - x_3 = c\,t$,

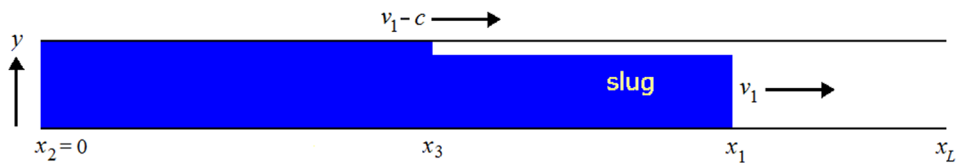

Fig. 8 Sketch of pipe filling. CV = slug = liquid volume between x_2 and x_1.

$$\int_{x_2}^{x_1(t)} \frac{\partial v}{\partial t}(x,t)\,\mathrm{d}x - \beta \int_{x_3(t)}^{x_1(t)} \frac{\partial v}{\partial t}(x,t)\,\mathrm{d}x$$
$$= v_2^2(t) - (1-\beta)\,v_1^2(t) - v_2(t)\frac{\mathrm{d}x_3}{\mathrm{d}t}(t) + (1-\beta)\,v_1(t)\frac{\mathrm{d}x_3}{\mathrm{d}t}(t)$$
$$+\frac{P_2(t)-P_1(t)}{\rho} + g\left[z(x_2) - z(x_1(t))\right] - \beta\, g\left[z(x_3(t)) - z(x_1(t))\right]$$
$$-\frac{f_2}{2D}\left(x_1(t) - c\,t\right)v_2^2(t) - \frac{f_1}{2D_H}\,c\,t\,(1-\beta)\,v_1^2(t) - \frac{K}{2}\,\rho A\,v_2^2(t)$$

or, using Eq. (22) and $x_1(t) = L(t)$ (Fig. 8) and the simplifications $f = f_1 = f_2$ and $D_H = D$

$$\int_{x_2}^{x_1(t)} \frac{\partial v}{\partial t}(x,t)\,\mathrm{d}x - \beta \int_{x_3(t)}^{x_1(t)} \frac{\partial v}{\partial t}(x,t)\,\mathrm{d}x$$
$$= (v_1(t) - \beta\,c)^2 - (1-\beta)\,v_1^2(t) - \beta\,(v_1(t) - c)^2$$
$$+\frac{P_2(t)-P_1(t)}{\rho} + g\left[z(x_2) - z(x_1(t))\right] - \beta\, g\left[z(x_3(t)) - z(x_1(t))\right]$$
$$-\frac{f}{2D}\left[L(t)\,(v_1(t) - \beta\,c)^2 - \beta\,c\,t\,(v_1(t) - c)^2 + \beta\,(1-\beta)\,c^3\,t\right]$$
$$-\frac{K}{2}\,\rho A\,(v_1(t) - \beta\,c)^2 \tag{27}$$

The remaining integral in Eq. (27) is approximated in the Appendix [Eq. (A2)], using $(\mathrm{d}v_1/\mathrm{d}t) = (\mathrm{d}v_2/\mathrm{d}t) = \left(\mathrm{d}^2x_3/\mathrm{d}t^2\right)$ [see Eq. (23) and above], because $\mathrm{d}c/\mathrm{d}t = 0$.

The governing equations in terms of v_1 and L are

$$(L(t) - \beta\,c\,t)\,\frac{\mathrm{d}v_1}{\mathrm{d}t}(t) = \underbrace{-\beta\,(1-\beta)\,c^2}_{+F_{\mathrm{air}}=0} + \frac{P_2(t)-P_1(t)}{\rho}$$
$$+g\left[z(x_2) - z(x_1(t))\right] - \beta\, g\left[z(x_1(t) - c\,t) - z(x_1(t))\right]$$
$$-\frac{f}{2D}\left[L(t)\,(v_1(t) - \beta\,c)^2 - \beta\,c\,t\,(v_1(t) - c)^2 + \beta\,(1-\beta)\,c^3\,t\right]$$
$$-\frac{K}{2}\,(v_1(t) - \beta\,c)^2 \tag{28}$$

where $x_3(t) = x_1(t) - c\,t$ has been used, and

$$\frac{\mathrm{d}L}{\mathrm{d}t}(t) = v_1(t) \tag{29}$$

To maintain a steady flow ($\mathrm{d}v_1/\mathrm{d}t \equiv 0$) when there is no force at all ($P_2 - P_1 = 0$, $g = 0$, $f = 0$ and $K = 0$), an additional term is needed that corresponds to the force [using Eq. (24)]

$$F_{\mathrm{air}} = \beta\,(1-\beta)\,c^2\,\rho A = \beta\,\rho\,g\,\cos\theta\,\frac{(1-\beta)^2\,A^2}{T} \tag{30}$$

Note that for a closed upstream end the flow is steady at $v_1 = \beta\,c$. The provisional assumption is now made that the air-driving force F_{air} is always there, so that the first term on the right-hand side of Eq. (28) cancels. Note that the chosen CV does *not* lose or gain mass at its two fronts.

The pressure in the rigid liquid column ($x < x_1(t)$) and in the free air ($x > x_1(t)$) are given by (it is inconsistent, but for simplicity the pressure of the intruded air is taken equal to $P_1(t)$)

$$P(x,t) = \begin{cases} P_2(t) + \dfrac{x - x_2}{L(t)}\left(P_2(t) - \dfrac{K}{2}\,\rho\,(v_1(t) - \beta\,c)^2 - P_1(t)\right) \\ \qquad \text{if } 0 = x_2 \le x \le x_1(t) \\ P_1(t) \text{ if } x_1(t) < x \le x_L \end{cases} \tag{31}$$

Analytical Solution. Analytical solutions are derived for the case $\beta = 0$ (no air intake, hence $c = 0$ and $v_1 = v_2$) when both the pressure difference $P_2 - P_1 > 0$ and the pipe slope $\theta > 0$ are constant. For filling from a reservoir with constant head H_R into an empty pipe ($P_1 = 0$), the governing equations are Eqs. (29) and (28) reduced to

$$L(t)\,\frac{\mathrm{d}v_1}{\mathrm{d}t}(t) = g\,H_R + g\,\sin\theta\,L(t) - \frac{f}{2D}\,L(t)\,v_1^2(t) - \frac{K+1}{2}\,v_1^2(t) \tag{32}$$

where $P_2(t) - P_1(t) = \rho\,g\,H_R$ and the $K+1$ term accounts for entrance loss and lost velocity head [4,5]. With $\mathrm{d}L/\mathrm{d}t := w(L) > 0$ and $C_2 := f/2D$, the following linear first-order ODE in w^2 is derived

$$\frac{\mathrm{d}w^2}{\mathrm{d}L} + \left(\frac{K+1}{L} + 2\,C_2\right)w^2 = \frac{2\,g\,H_R}{L} + 2\,g\,\sin\theta \tag{33}$$

The semi-analytical solution for initial conditions $v_1(t_0) = 0$ [or $w(L_0) = 0$] and $L(t_0) = L_0 > 0$ is obtained after multiplying Eq. (33) with the integrating factor $L^{K+1} + \mathrm{e}^{2C_2L}$

$$v_1 = L^{-\frac{K+1}{2}}\,\mathrm{e}^{-C_2L}\,\sqrt{2\,g}$$
$$\sqrt{H_R\int_{L_0}^{L} L^{*K}\,\mathrm{e}^{2C_2L^*}\,\mathrm{d}L^* + \sin\theta\int_{L_0}^{L} L^{*K+1}\,\mathrm{e}^{2C_2L^*}\,\mathrm{d}L^*} \tag{34}$$

The slug length L can be replaced by $L_0 + L_{\mathrm{pipe}}$, where L_{pipe} is the distance traveled by the slug front. This notation is adapted from Ref. [1].

The special case $K + 1 = 0$ (and $\beta = 0$) gives the solution

$$v_1 = \mathrm{e}^{-C_2L}\,\sqrt{2\,g}\,\sqrt{H_R\int_{L_0}^{L}\frac{\mathrm{e}^{2C_2L^*}}{L^*}\,\mathrm{d}L^* + \frac{\sin\theta}{2\,C_2}\left(\mathrm{e}^{2C_2L} - \mathrm{e}^{2C_2L_0}\right)} \tag{35}$$

The special case $f = 0$ (and $\beta = 0$) gives the solution

$$v_1 = \sqrt{2\,g}\,\sqrt{\frac{H_R}{K+1}\left(1 - \left(\frac{L_0}{L}\right)^{K+1}\right) + \frac{\sin\theta}{K+2}\,L\left(1 - \left(\frac{L_0}{L}\right)^{K+2}\right)} \tag{36}$$

with limit value $v_{1,\infty} = \sqrt{2\,g\,H_R/(K+1)}$ when $\theta = 0$.

For $K = 0$ and $\theta = 0$ (and $f = 0$ and $\beta = 0$) the arrival time of the slug front as a function of its distance traveled ($L_{\mathrm{pipe}} = L - L_0$) is obtained from Eqs. (36) and (29) as

$$\sqrt{2\,g\,H_R}\;(t - t_0) = L\,\sqrt{1 - \frac{L_0}{L}} + L_0\,\mathrm{artanh}\left(1 - \frac{L_0}{L}\right) \tag{37}$$

or in terms of the average slug speed, using $L = L_0 + L_{\mathrm{pipe}}$

$$\bar{v}_1 = \frac{L_{\mathrm{pipe}}}{t - t_0} = \frac{\sqrt{2\,g\,H_R}}{\sqrt{1 + L_0/L_{\mathrm{pipe}}} + \dfrac{L_0}{L_{\mathrm{pipe}}}\,\mathrm{artanh}\left(\dfrac{1}{1 + L_0/L_{\mathrm{pipe}}}\right)} \tag{38}$$

with limit value $\bar{v}_{1,\infty} = \sqrt{2\,g\,H_R}$.

Numerical Solution. Numerical integration is required when either the pressure difference $P_2 - P_1$ or the pipe slope θ is not constant. The governing equations (28) and (29) and $(\mathrm{d}x_1/\mathrm{d}t)(t) = v_1(t)$ can be casted in the standard form

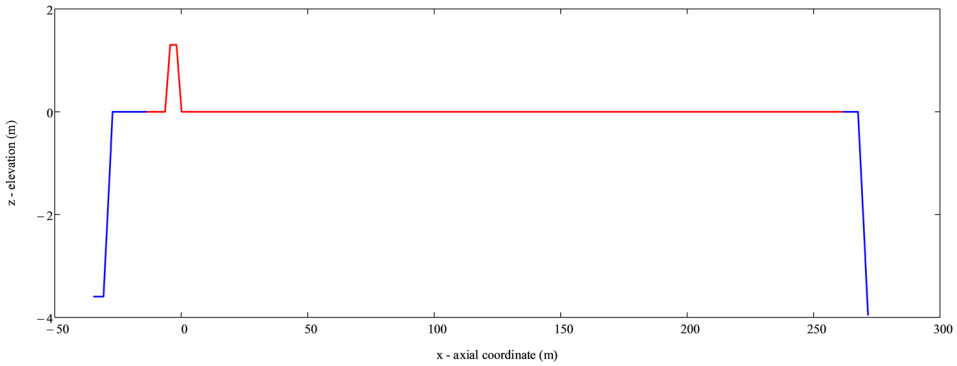

Fig. 9 Pipeline axial coordinates and elevation profile $z(x)$ for pipe filling [4]; not to scale

$$\frac{\mathrm{d}\boldsymbol{y}}{\mathrm{d}t} = \boldsymbol{f}(t, \boldsymbol{y}), \text{ with } \boldsymbol{y} := \begin{pmatrix} v_1 \\ L \\ x_1 \end{pmatrix} \tag{39}$$

The explicit Euler method is used herein to solve Eq. (39). The advantage of the current method is that spatial discretization and front tracking, such as in Refs. [4] and [5], are not needed.

Pipe-Filling Validation

Test Problem. The experimental setup described in Ref. [4] is used as test problem for pipe filling. The pipeline consists again of 275.2 m of PVC pipe of 0.2354 m diameter, but now it is connected to a water tower via a 20.6 -m-long steel supply line (the ignored side-branch in pipe emptying) of 0.2 m diameter. The water tower consists of a high tank and a vertical steel pipe below it. The tank has its free surface at an elevation of 24.25 m above the connection to the 0.2-m-diameter steel pipe and maintains a constant depth of 2 m. The vertical pipe is 22.25 m long and has a diameter of 1.0 m. The accelerations in this pipe are ignored in the simulations [17]. The inlet in the model is taken just upstream of valve V8 in Fig. 3 at $x = -34.6$ m, $z = -3.6$ m, adapted from Ref. [4], and as such includes 0.4 m of 1.0-m-diameter pipe and a diffuser of 1.0 m length. The pipeline elevation profile is shown in Fig. 9. The side-branch leading to the check valve and air tank is ignored in pipe filling. It is assumed to be free of air, since small-size air valves just downstream of the check valve were utilized to let any trapped air escape. The downstream valves V4 and V5 at $x = 271.0$ m and $x = 271.6$ m are fully open all the time. A stationary water-column of 28.1 m length starts to accelerate after suddenly opening the upstream valve V2 at $x = -29.9$ m. The input parameters for the numerical simulations are directly taken from Ref. [4], except a slightly modified H_R, and listed in Table 3. The length of the pipeline is taken up to the last and downward bend at $x = 267.0$ m, because the filling process is considered ended when the slug front hits this bend thereby causing violent vibrations and fluid-structure interaction [4]. The value of 0.13 for the air-intrusion coefficient β defines the thickness of the air layer and corresponds to an observed water depth h of 0.192 m, so that $h/D = 0.82$; see Fig. 4. The value $c = 1.43$ m/s is taken from Appendix I in Ref. [4]. The three valves V8, V0, and V2 indicated in Fig. 3, and a flow straightener and a perforated plate in the water tower (not shown) cause a significant head loss in the steel supply line. From the steady-state hydraulic grade line (Fig. 3 in Ref. [4]), the estimated head loss is $H_{\text{loss}} = 8.15$ m. This gives $K + 1 = 2gH_{\text{loss}}/v_\infty^2 = 10.0$ for $v_\infty = 4.0$ m/s (Fig. 5 in Ref. [4]) and includes the lost velocity head [4,5]. The pipeline was not entirely empty before filling it and initial water levels up to 0.035 m existed locally. This fact is entirely ignored in the numerical simulation, because pick-up has not been modeled.

Results

All analytical solutions have been successfully verified against numerical results and vice versa (not shown). The filling is rapid and takes place within one minute time. The initial acceleration from rest at $t = t_0 = 0$ according to Eq. (28) is

$$\psi \frac{\mathrm{d}v_1}{\mathrm{d}t}(0) = \frac{g}{L_0}\left\{H_R + \left[z(x_2(0)) - z(x_1)\right]\right\} \tag{40}$$

where ψ is an unsteady friction coefficient ($1 \le \psi \le 4/3$) and the initial difference in elevation between water–air front and the inlet is $z(x_2(0)) - z(x_1) = -3.6$ m. With $H_R = 24.25$ m and $\psi = 4/3$ this yields an acceleration of 5.4 m/s^2 and a value of $\mathrm{d}Q/\mathrm{d}t = 0.23$ m^3/s^2. The calculated and measured flow rates are shown in Fig. 10(*a*), where the current calculation is based on Eq. (28) (with H_R and K as input and the added factor $\psi = 4/3$), whereas the calculation in Ref. [4] was based on the pressure history measured at $x = -14$ m so that the entire upstream steel section could be ignored. After a very quick acceleration (a velocity of 5.9 m/s is reached within 2.8 s time in the experiment) to its maximum, the flow rate gradually decreases because of the increasing slug length (and thus increasing inertia and skin friction). The fast acceleration and slow deceleration make the flow history roughly bilinear with its maximum at the intersection of two nearly straight lines. It would be nice if this maximum could be estimated in advance from one of the analytical solutions. In the experiment the leading water front arrives at the outflow flowmeter at $x = 270.3$ m after about 54 s at a speed of 4.0 m/s. In the simulation, water arrives at the bend at $x = 267.0$ m after 57 s at a speed of 4.1 m/s. There is not a big influence of air

Table 3 Input data for pipe-filling simulations

Input parameters	Notation	Values
Length of pipeline up to last bend	x_L	301.6 m
Initial slug length	L_0	28.1 m
Average diameter of pipeline	D	0.233 m
Mass density of water	ρ	998.5 kg/m^3
Gravitational acceleration	g	9.81 m/s^2
Friction factor (PVC pipe)	f	0.0136
Entrance and valves' loss coefficient	$K+1$	10.0
Air intrusion coefficient	β	0.13
Air intrusion speed	c	1.43 m/s
Reservoir pressure head	H_R	24.25 m
Elevation profile	$z(x)$	see Fig. 9
Derived quantities	**Notation**	**Values**
Flow area	A	0.0426 m^2
Initial mass	m_0	12838 kg
$f/(2D)$	C_2	0.0292 1/m

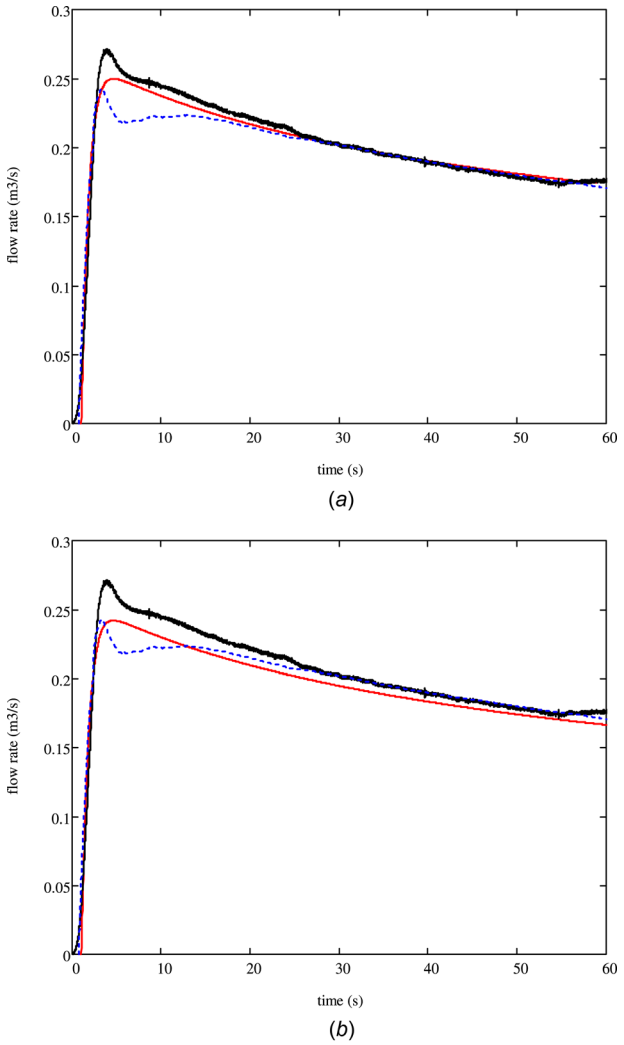

Fig. 10 Outflow discharges in pipe filling: (*a*) $\beta = 0.13$, (*b*) $\beta = 0$ (no air intrusion). Measured (continuous line with highest peak) [4], calculated herein (continuous line), and calculated in Ref. [4] (discontinuous line).

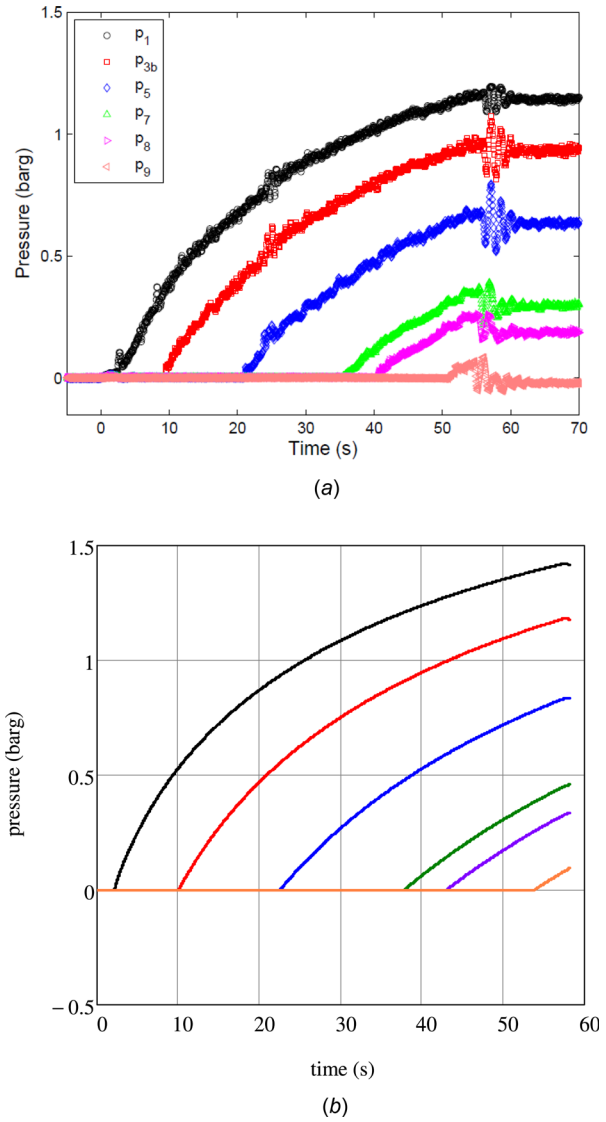

Fig. 11 Pressure histories at measurement Sections 1, 3, 5, 7, 8, and 9 for pipe filling: (*a*) measured [4] and (*b*) calculated

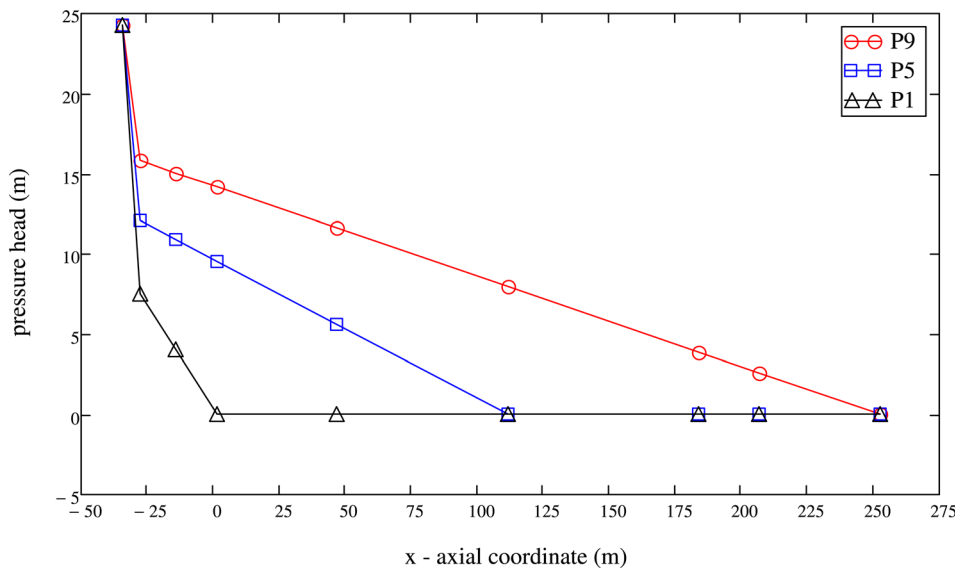

Fig. 12 Pressure-head distributions in pipe-filling simulation at the instant that the water front arrives at Sections 1 (Δ), 5 (□), and 9 (○)

intrusion when comparing Figs. 10(*a*) (with) and 10(*b*) (without intrusion), as already stated in Ref. [4], because β is small. The actual (average) value of β can be estimated from pipeline volume minus supplied volume, if the pipeline were initially entirely empty, which unfortunately was not the case.

The measured and calculated pressure histories at Sections 1, 3, 5, 7, 8, and 9 (see Fig. 3) are shown in Fig. 11. The simulated trends in Fig. 11(*b*) are right, but the magnitudes are systematically too large, probably because the pipeline was not entirely empty in the experiment. Figure 12 displays the calculated pressure-head distributions when the first water arrives successively at Sections 1, 5 and 9 (see Fig. 3), thereby noting that the corresponding Fig. 3 in Ref. [4] is not entirely correct. The upstream pressure drop is due to resistance and decreases with decreasing velocity. The gradient of the pressure head in the rigid column is constant by definition.

Conclusion

Refined 1D models for rapid emptying and filling of pipelines have been derived in which the 3D effects of holdup and air intrusion are included in a global way. Full analytical solutions have been found for the case that the driving pressure and the slope of the pipeline are constant. Analytical solutions for several limit cases give useful insight in the underlying mechanisms and they allow a theoretical parameter-sensitivity analysis. All closed-form solutions and corresponding numerical solutions have been successfully verified against each other. The proposed numerical method has the advantage that spatial discretization and front tracking are not needed. The derived models were able to predict the right trends and magnitudes in flow rates and pressures measured in a large-scale pipeline apparatus. The influence of holdup in the emptying experiment and air intrusion in the filling experiment were both significant. Emptying and filling times, flow rates and pressure distributions, can be predicted with acceptable accuracy with the proposed 1D models. The mathematical models and corresponding simulations were also essential for a correct interpretation and understanding of the laboratory experiments.

Acknowledgment

This paper is inspired by Paper No. 28693 presented at the ASME PVP2014 conference held in Anaheim, California. The second author is grateful for the support by the National Natural Science Foundation of China (No. 51478305), Scientific Research Foundation for the Returned Overseas Chinese Scholars, State Education Ministry, and SKL of HESS (HESS-1408).

Nomenclature

a = pressure wave speed (m/s)
A = cross-sectional pipe area (m^2)
A_l = cross-sectional flow area (m^2)
c = air intrusion speed (m/s)
C = constant
$C_2 = f/(2D)$ (1/m)
CV = control volume
D = inner pipe diameter (m)
e = exponential function
Ei = exponential integral
EMF = electromagnetic flowmeter
f = Darcy–Weisbach friction coefficient
$\boldsymbol{f}$ = vector function
$\tilde{f}$ = constant (1/m)
f^* = constant (1/m)
f_0 = waterhammer frequency (Hz)
g = acceleration due to gravity (m/s^2)
h = liquid flow depth (m)
H = pressure head (m)
K = entrance or exit loss coefficient
L = length of slug (m)
L_{pipe} = distance traveled by slug front or tail (m)
L^* = dummy length in integral (m)
m = mass of slug (kg)
P = pressure (Pa)
Q = flow rate (m^3/s)
t = time (s)
T = top width of flow section (m)
v = velocity (m/s)
V = volume (m^3)
w = time derivative of L (m/s)
x = axial position (m)
x_L = pipe length (m)
$\boldsymbol{y}$ = vector of unknowns
z = pipeline elevation (m)
β = holdup coefficient in pipe emptying; air-intrusion coefficient in pipe filling
γ = constant
Γ = incomplete gamma function
Γ^* = self-defined function
Δ = step (in time or space)
$\Delta P = P_2 - P_1$ (Pa)
θ = angle of downward inclination of pipe (rad)
λ = dummy parameter
ρ = mass density of liquid (kg/m^3)
τ = travel time (s)
ψ = unsteady friction coefficient

Subscripts

H = hydraulic
hu = holdup
l = liquid
R = reservoir
wh = waterhammer
0 = initial value; constant value
1 = slug front
2 = slug tail
3 = air intrusion front
∞ = final value

Appendix: Approximation of Integrals

The three integrals appearing in Eq. (8) are evaluated below.

The gravity term can be calculated exactly, because $\sin\theta = -\mathrm{d}z/\mathrm{d}x$

$$-\int_{x_2(t)}^{x_1(t)} \sin\theta(x)\,\mathrm{d}x = z(x_1(t)) - z(x_2(t)) \tag{A1}$$

where z is the continuous pipeline elevation.

The two remaining integrals in Eq. (8) are approximated. Assuming that the velocity increases linearly from v_1 at x_1 to v_2 at x_2 yields

$$\begin{aligned}\int_{x_2(t)}^{x_1(t)} \frac{\partial v}{\partial t}(x,t)\,\mathrm{d}x &\approx \frac{1}{2}\left(\frac{\partial v}{\partial t}\left(x_1^-(t),t\right) + \frac{\partial v}{\partial t}\left(x_2^+(t),t\right)\right)\left(x_1(t) - x_2(t)\right)\\ &= \frac{1}{2}\left(\frac{\mathrm{d}v_1}{\mathrm{d}t}(t) + \frac{\mathrm{d}v_2}{\mathrm{d}t}(t)\right)\left(x_1(t) - x_2(t)\right)\\ &= \frac{1-\frac{1}{2}\beta}{1-\beta}\,L(t)\,\frac{\mathrm{d}v_1}{\mathrm{d}t}(t)\\ &= \left(1-\frac{1}{2}\beta\right)L(t)\,\frac{\mathrm{d}v_2}{\mathrm{d}t}(t)\end{aligned} \tag{A2}$$

and

$$\int_{x_2(t)}^{x_1(t)} v^2(x,t)\,\mathrm{d}x \approx \frac{1}{3}\left(v^2(x_1^-(t),t) + v(x_1^-(t),t)\,v(x_2^+(t),t) + v^2(x_2^+(t),t)\right)\left(x_1(t)-x_2(t)\right)$$
$$= \frac{1}{3}\left(v_1^2(t) + v_1(t)\,v_2(t) + v_2^2(t)\right)\left(x_1(t)-x_2(t)\right)$$
$$= \frac{1-\beta+\frac{1}{3}\beta^2}{(1-\beta)^2}\,L(t)\,v_1^2(t)$$
$$= \left(1-\beta+\frac{1}{3}\beta^2\right)L(t)\,v_2^2(t) \tag{A3}$$

References

[1] Tijsseling, A. S., Hou, Q., and Bozkuş, Z., 2016, "An Improved One-Dimensional Model for Liquid Slugs Traveling in Pipelines," ASME J. Pressure Vessel Technol., **138**(1), p. 011301.

[2] Hou, Q., Tijsseling, A. S., and Bozkuş, Z., 2014, "Dynamic Force on an Elbow Caused by a Traveling Liquid Slug," ASME J. Pressure Vessel Technol., **136**(3), p. 031302.

[3] Laanearu, J., Annus, I., Koppel, T., Bergant, A., Vučkovič, S., Hou, Q., Tijsseling, A. S., Anderson, A., and van't Westende, J. M. C., 2012, "Emptying of Large-Scale Pipeline by Pressurized Air," ASCE J. Hydraul. Eng., **138**(12), pp. 1090–1100.

[4] Hou, Q., Tijsseling, A. S., Laanearu, J., Annus, I., Koppel, T., Bergant, A., Vučkovič, S., Anderson, A., and van't Westende, J. M. C., 2014, "Experimental Investigation on Rapid Filling of a Large-Scale Pipeline," ASCE J. Hydraul. Eng., **140**(11), p. 04014053.

[5] Liou, C. P., and Hunt, W. A., 1996, "Filling of Pipelines With Undulating Elevation Profiles," ASCE J. Hydraul. Eng., **122**(10), pp. 534–539. (Discussion and Closure: 123(12), pp. 1170–1174).

[6] Vasconcelos, J. G., and Wright, S. J., 2008, "Rapid Flow Startup in Horizontal Pipelines," ASCE J. Hydraul. Eng., **134**(7), pp. 984–992.

[7] Laanearu, J., Hou, Q., Annus, A., and Tijsseling, A. S., 2015, "Water-Column Mass Losses During Emptying of a Large-Scale Pipeline by Pressurized Air," Proc. Est. Acad. Sci., **64**(1), pp. 8–16.

[8] Bergant, A., Hou, Q., Keramat, A., and Tijsseling, A. S., 2011, "Experimental and Numerical Analysis of Water Hammer in a Large-Scale PVC Pipeline Apparatus," 4th IAHR International Meeting on Cavitation and Dynamic Problems in Hydraulic Machinery and Systems, A. Gajic, M. Benisek, and M. Nedeljkovic, eds., Belgrade, Serbia, pp. 27–36.

[9] Bergant, A., Hou, Q., Keramat, A., and Tijsseling, A. S., 2013, "Waterhammer Tests in a Long PVC Pipeline With Short Steel End Sections," J. Hydraul. Struct., **1**(1), pp. 23–34.

[10] Koppel, T., and Ainola, L., 2006, "Identification of Transition to Turbulence in a Highly Accelerated Start-Up Pipe Flow," ASME J. Fluids Eng., **128**(4), pp. 680–686.

[11] Kruisbrink, A., Ch., H., and Tijsseling, A. S., 2008, "The Momentum Flux Coefficient for Modelling Steady and Unsteady Head Losses in Turbulent Pipe Flow," 10th International Conference on Pressure Surges, S. Hunt, ed., Edinburgh, UK, BHR Group, Cranfield, UK, pp. 379–399.

[12] He, S., Ariyaratne, C., and Vardy, A. E., 2008, "A Computational Study of Wall Friction and Turbulence Dynamics in Accelerating Pipe Flows," Comput. Fluids, **37**(6), pp. 674–689.

[13] He, S., Ariyaratne, C., and Vardy, A. E., 2011, "Wall Shear Stress in Accelerating Turbulent Pipe Flow," J. Fluid Mech., **685**, pp. 440–460.

[14] Annus, I., Koppel, T., Sarv, L., and Ainola, L., 2013, "Development of Accelerating Pipe Flow Starting From Rest," ASME J. Fluids Eng., **135**(11), p. 111204.

[15] Tijsseling, A. S., and Vardy, A. E., 2008, "Time Scales and FSI in Oscillatory Liquid-Filled Pipe Flow," 10th International Conference on Pressure Surges, S. Hunt, ed., Edinburgh, UK, BHR Group, Cranfield, UK, pp. 553–568.

[16] Wiggert, D. C., 1972, "Transient Flow in Free-Surface, Pressurized Systems," ASCE J. Hydraul. Division, **98**(1), pp. 11–27.

[17] Tijsseling, A. S., Hou, Q., Svingen, B., and Bergant, A., 2012, "Acoustic Resonance in a Reservoir-Double Pipe-Orifice System," ASME Paper No. PVP2012-78085.